Effect of Heat Treatments on *In-Situ* $Al_2O_3/TiAl_3$ Composites Produced from Squeeze Casting of TiO_2/A356 Composites

CHIA-WEN HSU and CHUEN-GUANG CHAO

In-situ $Al_2O_3/TiAl_3$ intermetallic matrix composites were fabricated *via* squeeze casting of TiO_2/A356 composites heated in the temperature range from 700 °C to 780 °C for 2 hours. The phase transformation in TiO_2/A356 composites employing various heat-treatment temperatures (700 °C to 780 °C) was studied by means of differential thermal analysis (DTA), microhardness, scanning electron microscopy (SEM), electron probe microanalysis (EPMA), and X-ray diffraction (XRD). From DTA, two exothermic peaks from 600 °C to 750 °C were found in the TiO_2/A356 composites. The XRD showed that Al_2O_3 and $TiAl_3$ were the primary products after heat treatment of the TiO_2/A356 composite. The fabrication of *in-situ* $Al_2O_3/TiAl_3$ composites required 33 vol pct TiO_2 in Al and heat treatment in the range from 750 °C to 780 °C. The hardness (HV) of the *in-situ* $Al_2O_3/TiAl_3$ composites (1000 HV) was superior to that of nonreacted TiO_2/A356 composites (200 HV). However, the bending strength decreased from 685 MPa for TiO_2/A356 composites to 250 MPa for $Al_2O_3/TiAl_3$ composites. It decreased rapidly because pores occurred during the formation of Al_2O_3 and $TiAl_3$. The activation energy of the formation of Al_2O_3 and $TiAl_3$ from TiO_2 and A356 was determined to be about 286 kJ/mole.

I. INTRODUCTION

INTERMETALLIC compounds have been considered for a wide range of high temperatures, and much research effort has been devoted to their development in the last ten years. The Ti-aluminides are prime candidates for high-temperature applications such as aircraft turbine engines, the space shuttle, and others.[1] The ordered intermetallic compounds $Ti_3Al(\alpha_2)$, $TiAl(\gamma)$, and $TiAl_3(\eta)$ have an attractive combination of properties such as a low density, high elastic modulus, high melting temperature, and good oxidation resistance.[2,3] However, these materials have poor creep resistance and poor room-temperature toughness. Intermetallic matrix composites (IMCs) may provide the right combination of high-temperature strength, creep resistance, and environmental stability with adequate ambient-temperature ductility and low density. DiPietro *et al.*[4] have reported on the compressive properties of TiB_2 particulate composites with $TiAl_3$ as a matrix. Below 600 °C, the strength-to-density ratio has been reported to be approximately 4 times that for superalloys. These results imply that $TiAl_3$ is worthy of more extensive studies as a composite matrix.

Currently, a variety of methods have been applied to the fabrication of IMCs. Particulate-reinforced composites have been produced by powder mixing and consolidation,[5] liquid/particle cospraying,[6] and *in-situ* precipitation.[7] For example, Peng *et al.*,[8] using Al, TiO_2, and B powders, produced $TiAl_3$-Al_2O_3-TiB_2 composites by the XD process (The XD process is a liquid-solid reaction method of producing ceramic reinforcing in-situ particulate in a matrix). Welham[9] reported that TiO_2 and milled aluminum powder showed complete reaction to Al_2O_3 and $TiAl_3$ after heating to 600 °C, whereas the unmilled powder reaction was incomplete after 1 hour at 1200 °C. Some researchers produced $TiAl_3/Al_2O_3$ composites by squeeze casting, using TiO_2 powders as the reinforcement, molten pure aluminum as the matrix, and a process of reaction.[10] Two kinds of reaction methods were utilized. One method was to produce reaction squeeze-cast products through higher-temperature conditions of the squeeze-casting process.[11] The hardness of such samples was HV 300 to 1050.

However, it is difficult to make a uniform fine structure with the simple combination of aluminum and TiO_2. The other method involved producing nonreacted (TiO_2/Al) composites at lower-temperature conditions of the squeeze-casting process, and then, through subsequent heat treatments, allowing the reaction of TiO_2 and Al to occur. Isao Tsuchitori *et al.*[12] suggested that the hardness of a TiO_2/Al composite increased gradually during isothermal heat treatment (below the liquidus temperature). However, the maximum hardness (HV 765) of the composites after heat treatment was much lower than that (HV 1050) of the composite produced by reaction squeeze casting.

In the current work, the conventional squeeze-casting process was applied to the manufacture of TiO_2/A356 composites, and then these were heated to a temperature ranging from 700 °C to 780 °C (above the liquidus temperature) to form $TiAl_3/Al_2O_3$ composites. The correlation between the heat-treatment temperature and final equilibrium properties of the composites was also investigated by X-ray diffraction analysis (XRD), Vickers microhardness testing, electron probe X-ray microanalysis (EPMA), scanning electron microscopy (SEM), and testing for bend strength.

CHIA-WEN HSU, formerly Graduate Student, Institute of Materials Science and Engineering, National Chiao Tung University, is Senior Process Engineer, UMC, Hsinchu, Taiwan 30077, Republic of China. CHUEN-GUANG CHAO, Professor, is with the Department of Materials Science and Engineering, National Chiao Tung University, Hsinchu, Taiwan 30050, Republic of China.

Manuscript submitted April 28, 2000.

II. EXPERIMENTAL

The composite materials were produced by squeeze casting. The basis of the fabrication technique has been described in our previous study.[13] At first, TiO_2 anatase powders were shaped to the preform of a 50 × 50 mm square bar by a hydraulic press. Next, the cold-pressed TiO_2 preform was sintered in an air furnace at 1100 °C for 30 minutes. The preform was set into a preheated metal die and heated to a given temperature; then, the molten A356 aluminum alloy was squeezed by the punch at a certain pressure. The process conditions are listed in Table I. The specimens with 33 vol pct TiO_2 were heat treated in the air furnace at different temperatures ranging from 700 °C to 780 °C, with various time intervals from 180 seconds to 24 hours. For comparison, the specimens with 20 vol pct TiO_2 were prepared for XRD analysis. The physical properties of A356 and TiO_2 are listed in Table II.

Microstructural characterization was carried out by using light microscopy and SEM. The SEM was used to examine the morphology, and EPMA was carried out to identify the composition of the compound. Differential thermal analysis (DTA) was performed by using a DUPONT* 2100 thermal analyzer. The samples were cut to the approximate shape of 2 mm cube. The heating rate was 10 °C/min from 450 °C to 950 °C. Dry nitrogen was purged through the cell at the rate of 40 mL/min to avoid oxidation. Phase identification was conducted by a SEIMENS** D5000 X-ray diffractometer with nickel-filtered Cu K_α radiation, scanning at a speed of 0.02 deg and a step time of 2 seconds. A Vickers hardness (HV) measurement of heat-treated specimens was made using a diamond pyramid indenter and a 500 g load. According to JIS R1601 (Figure 1) specification, the three-point bending test was employed to measure the strength of the composites. The test machine was an Instron 8501, with a 0.01 mm/min compression rate to measure the bending strength. For each heat-treated condition, we took eight specimens to obtain the average value. The bending strength (σ_b) was determined from

$$\sigma_b \text{ (MPa)} = 3 \times P \times L/2 \times W \times t^2$$

where L is the length, W is the width, P is the load, and t is the thickness.[14]

*DUPONT is a trademark of DuPont de Nemours & Co., Inc., Wilmington, DE.

**SIEMENS is a trademark of Siemens.

Table I. Squeeze Casting Conditions

Molten Al Temperature (°C)	Mold Temperature (°C)	Preform Temperature (°C)	Squeeze Pressure (MPa)	Squeeze Time (s)
770	450	450	50	120

III. RESULTS

A. *DTA Analysis*

Figure 2(a) shows the DTA curves of a squeeze-cast TiO_2/A356 sample and an Al (A356) sample. The curve of A356 is well known, and it has two endothermic peaks at 585 °C and 625 °C, respectively. These two peaks represent the Al-Si eutectic temperature (585 °C) and liquidus temperature (625 °C) of the sample. There are three peaks presented in the curve of the TiO_2/A356 composite. An endothermic peak is found at 586.5 °C, which denotes the eutectic temperature of the aluminum alloy in the TiO_2/A356 composite. Instead of a second peak (625 °C), which represents the liquidus temperature of A356, two exothermic peaks are found. According to Peng *et al.*'s report,[8] a reaction process of TiO_2 and Al produces Al_2O_3 particles and [Ti] atoms.

$$3TiO_2 + 4Al \rightarrow 2Al_2O_3 + 3[Ti] \quad [1]$$

This exothermic reaction may raise the temperature to about 2000 °C, at which Al and Ti are a liquid state, but α-Al_2O_3 remains in the solid state. The liquid phase of Al-Ti subsequently reacts to form $TiAl_3$. These results suggest that the first exothermic peak (600 °C to 645 °C, with a maximum at 613.6 °C) is the formation of Al_2O_3 and the second one (680 °C to 750 °C, with a maximum at 731.9 °C) is the formation of $TiAl_3$. After heat treatment of the TiO_2/A356 composite at 780 °C for 2 hours, there is no peak observed from 450 °C to 900 °C, as shown in Figure 2(b). It means that Al has completely reacted with TiO_2.

B. *XRD Analysis*

For the specimen squeeze-cast without any heat treatment, only TiO_2, Al, and Si appeared; no other obvious peak was detected by the XRD pattern analysis shown in Figure 3. There is no obvious reaction between Al and TiO_2 caused by squeeze casting. This phenomenon was also verified by Suganuma *et al.*,[15] while Fukunaga *et al.*[10] reported that Al_2O_3 or some Al-Ti intermetallic compounds were found after squeeze casting. After heating at 720 °C for 2 hours, Al_2O_3 and $TiAl_3$ peaks appeared in the X-ray spectrum. TiO_2 peaks become weak or invisible. Al peaks still existed but become small. The XRD peaks of Al vanished in the specimen with 33 vol pct TiO_2 after heat treatment for 2 hours at a temperature greater than 740 °C. However, the specimen with 20 vol pct TiO_2 has XRD peaks of Al even after heat treatment to 1100 °C, as shown in Figure 4.

C. *Microstructure*

Figure 5 illustrates a typical microstructure of a TiO_2/A356 composite without heat treatment. It shows that the

Table II. The Physical Properties of A356 and TiO_2

Properties/ Materials	Density (g/cm^3)	Elastic Modulus (GPa)	CTE (ppm/K)	Hardness (HV)	Bending Strength (MPa)	Poisson's Ratio	Melting Temperature (°C)
A356	2.685	72	21 to 24	20	375	0.33	615
TiO_2	3.84	283	8.5 to 9.5	800	69 to 103	0.28	1830

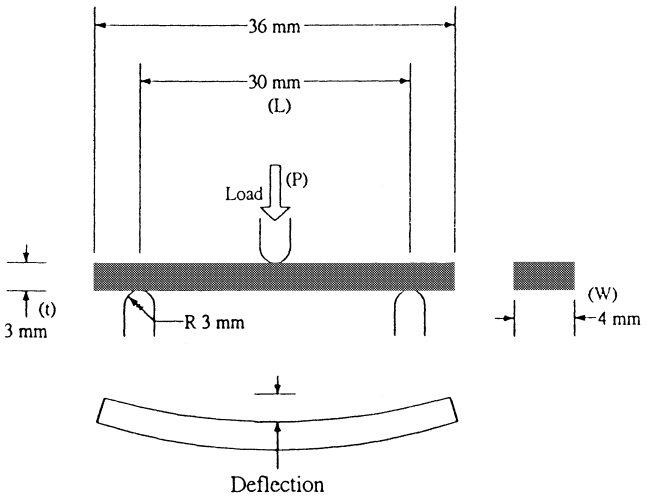

Fig. 1—The shape and size of the three-point bending test specimen.

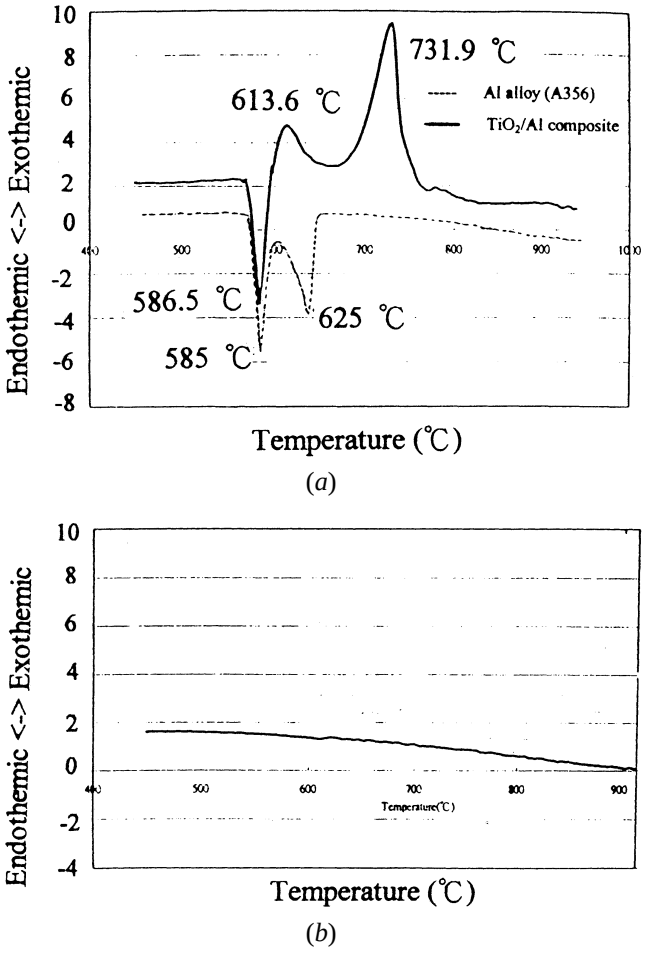

Fig. 2—(*a*) DTA of specimen Al alloy (A356) and TiO_2/A356 composite. (*b*) DTA of composite heated at 780 °C for 2 h.

dispersion of TiO_2 powder in the Al matrix is homogeneous. No obvious pores or clusters of TiO_2 powder are found. The results of a typical EPMA of the TiO_2/A356 composite are shown in Figure 6. The secondary electron image of the microstructure of the composite (the TiO_2 powder in the A356 matrix) is shown in Figure 6(a). Figures 6(b) through

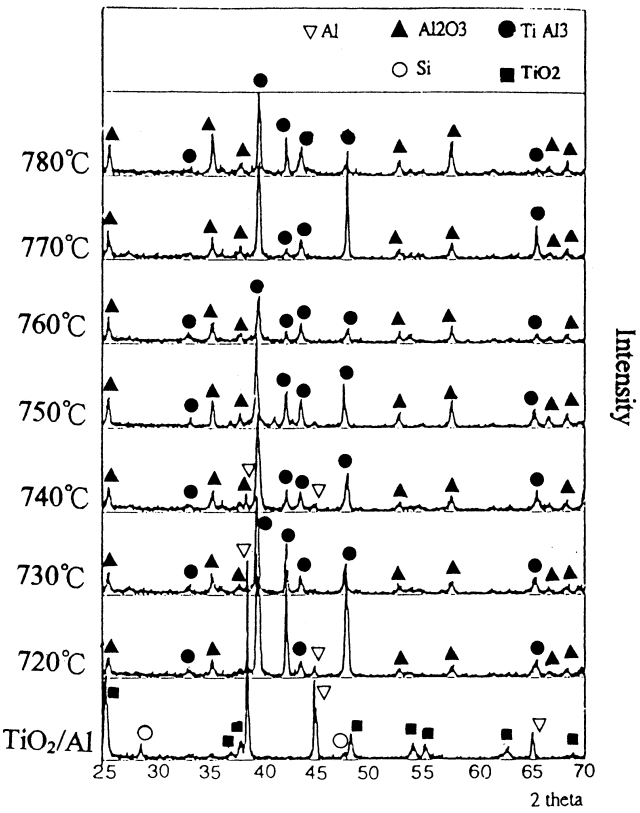

Fig. 3—XRD pattern of TiO_2/A356 composite with 33 vol pct TiO_2.

(e) indicate the corresponding X-ray images of Al, Ti, O, and Si, respectively. The Al X-ray image mapping represents the dispersion of Al in the matrix, and Ti X-ray image mapping represents the distribution of TiO_2 powder. For X-ray image mapping of the O element, it appears to be a homogenous distribution. This may explain why TiO_2 and Al_2O_3 are in the specimen shapes. The Si element is distributed in a striped pattern. This is an ordinary micromorphology of Al-Si eutectic phase in cast A356.

Figure 7 shows that the shape of reinforcements (products) is changed when the heat treatment was executed at 770 °C (higher than the melting point of the matrix). The products become bigger and round in shape. The results of a typical EPMA of a TiO_2/A356 composite after heating at 770 °C for 2 hours are shown in Figure 8. Owing to the generation of Al_2O_3 and $TiAl_3$ after heat treatment, Ti does not spread as homogeneously as Al. The O element X-ray image mapping shows a homogeneous distribution. This may explain why TiO_2 and Al_2O_3 particles are in the specimen before and after heat treatment. The Si element appears to have a homogeneous distribution. Because there is no silicon or silicon-compound peak in the X-ray spectrum after heat treatment, as shown in Figure 3, Si may be dissolved into the matrix. However, the Si effect on the reaction with TiO_2 in the heat-treatment process still needs further study. Figure 9 shows that the morphology of particles in the matrix, based on SEM observations, changed in shape and size. The irregular shapes of the TiO_2 powder, shown in Figure 9(a), were gradually transformed into round shapes of Al_2O_3, shown in Figures 9(b) and (c).

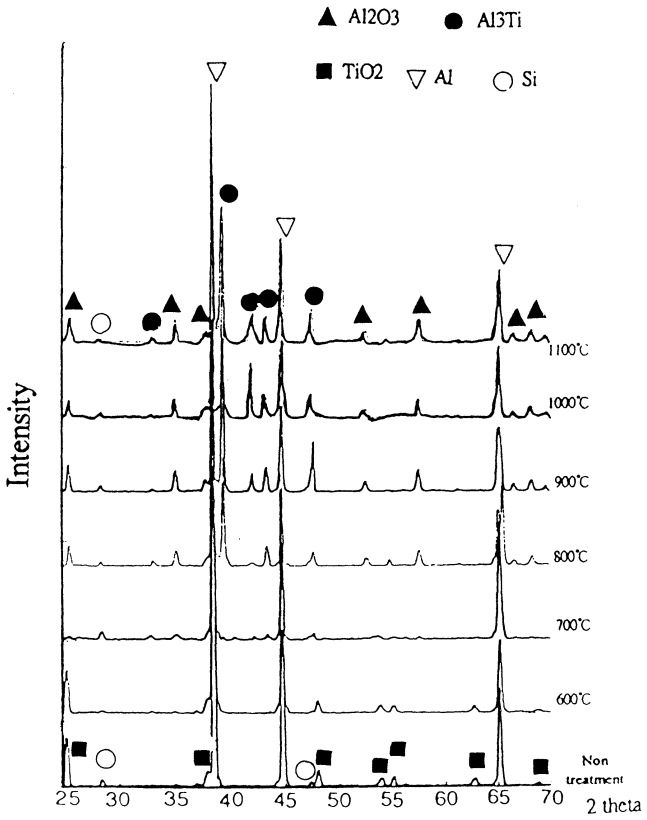

Fig. 4—XRD pattern of TiO_2/A356 composite with 20 vol pct TiO_2.

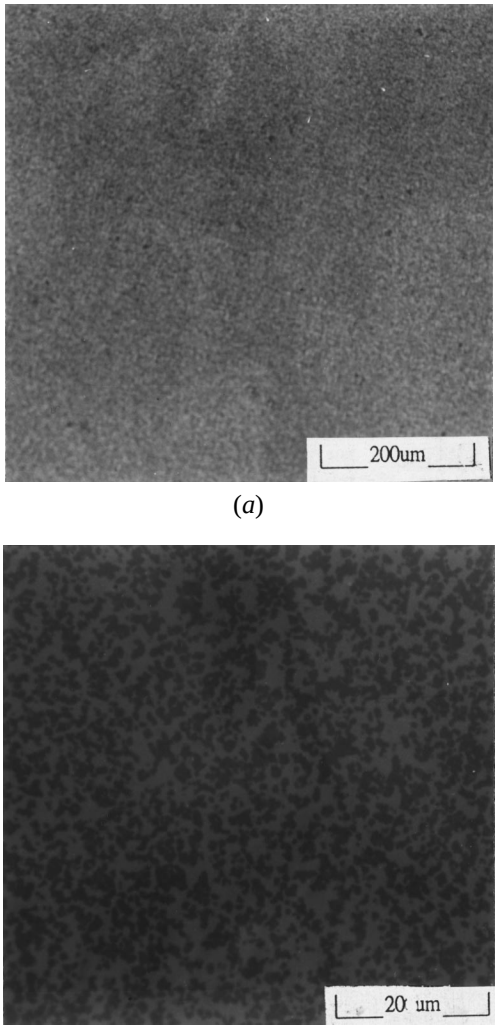

(*a*)

(*b*)

Fig. 5—(*a*) OM observation of TiO_2/A356 composite as-squeezed (without heat treatment). (*b*) Enlargement of (a).

D. *Hardness*

Figure 10 shows the pictorial drawing of hardness under different heat-treatment temperatures and times. The results of the hardness test can be divided into two groups by heat-treatment temperatures. One group, which was heat treated below 740 °C, has the lower maximum hardness of 725 HV; the other group, which was heat treated above 740 °C, has the higher maximum hardness of 1000 HV. The hardness increases with increasing heat-treatment time.

E. *Bending Test*

The bending strength with various temperatures is shown in Figure 11. The composite composed of TiO_2/A356 without heat treatment has an excellent bending strength (685 MPa). The lowest bending strength (154 MPa) occurs in the specimen heated at 700 °C for 2 hours, and a bending strength of about 180 to 250 MPa occurs with a heat-treatment temperature of 750 °C to 770 °C.

IV. DISCUSSION

From the results of Figure 3, the formation ofAl_2O_3 and $TiAl_3$ was found in specimens with 33 vol pct TiO_2 that were heat treated. The XRD peaks of Al vanished, and the primary XRD peaks were $TiAl_3$ and Al_2O_3 after the heat-treatment temperature over 740 °C. The same results are shown in Figure 2(a); the second exothermic reaction of TiO_2 and Al was finished at 750 °C in the DTA curve of the composites. However, the specimen with 20 vol pct TiO_2 has XRD peaks of Al even if heated to 1100 °C, as shown in Figure 4. According to the thermodynamics point of view, the following deoxidization reaction (Eq. [2]) can be written by considering the free-energy changes for possible reaction products between the TiO_2 reinforcement and the aluminum matrix[16,17,18] and the Al-Ti phase equilibrium diagram taken from Reference 19.

$$3TiO_2 + (13 + x)Al \rightarrow 3TiAl_3 + 2Al_2O_3 + xAl \quad [2]$$

A volume fraction of 33 vol pct TiO_2 leads to the complete reaction ($x = 0$) of $TiAl_3$ and Al_2O_3. Therefore, the Al phase still exists over 750 °C ($x > 0$) when the volume fraction of TiO_2 is lower than 33 pct.

After the heat treatment of TiO_2/Al composites, $TiAl_3$ and Al_2O_3 are produced. Because the products have a higher hardness than that of TiO_2 and Al, the composite is hardened by the reaction. The results of the hardness test can be divided into two groups by heat-treatment temperatures. One group is in the range from 720 °C to 740 °C; the other group is in the range from 750 °C to 780 °C. For the first group (720 °C to 740 °C), the hardness reaches its maximum of about 725 HV, since some Al still remains. The second group, with heat-treatment temperatures from 750 °C to 780

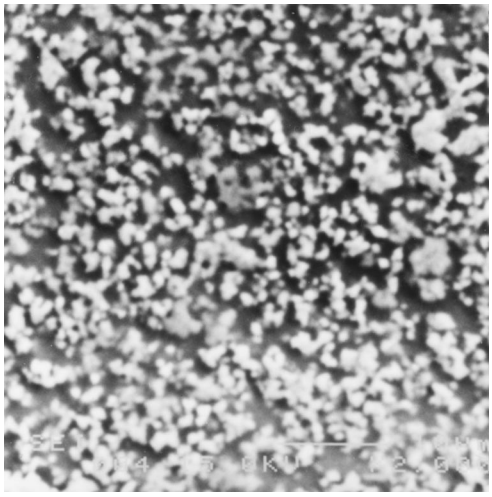

(*a*)

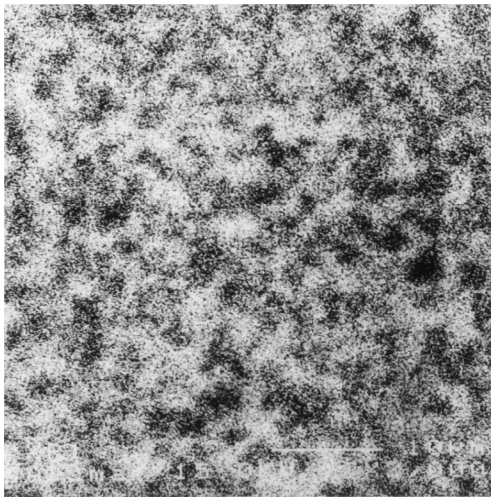

(*b*)

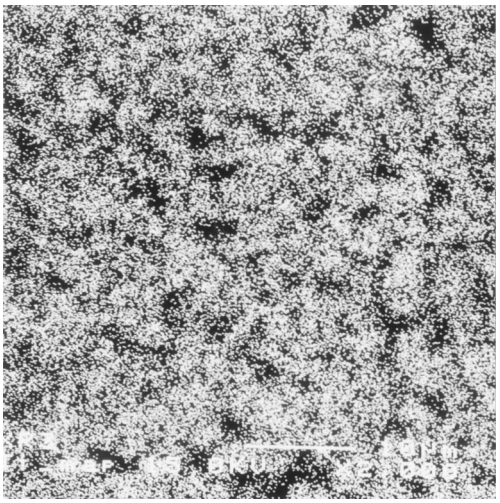

(*c*)

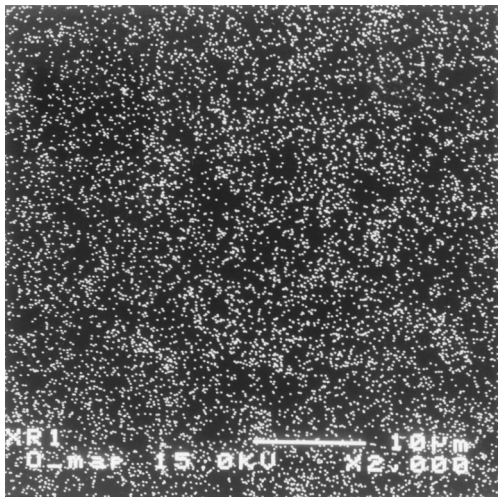

(*d*)

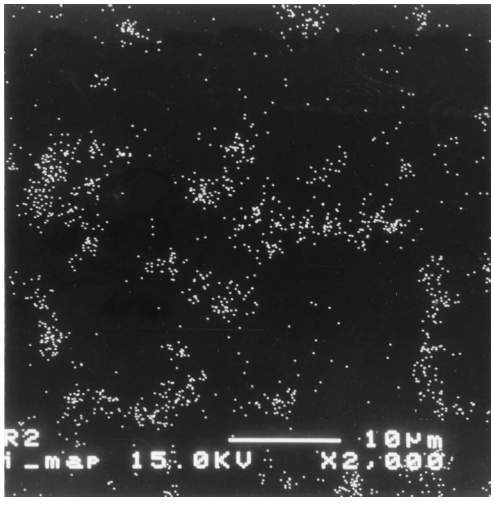

(*e*)

Fig. 6—EPMA of TiO_2/A356 composite as-squeezed, showing (*a*) the electron image of a region and corresponding X-ray images of (*b*) Al, (*c*) Ti, (*d*) O, and (*e*) Si.

°C has a higher hardness of up to 1000 HV, since the Al completely transforms. Some articles[20,21] use hardness to represent the reaction and give the correlation of reaction time and temperature. In the hardening reaction, the apparent activation energy can be calculated by different heat treatments.[22]

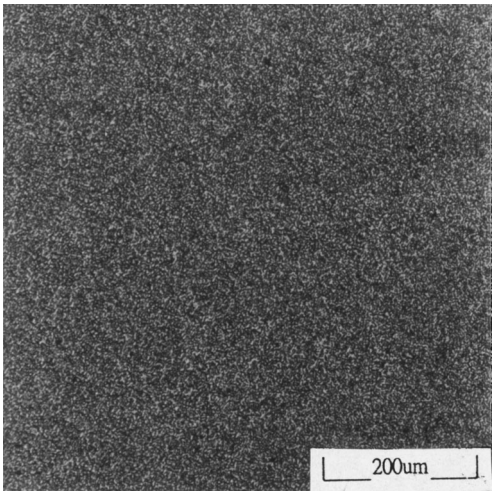

(*a*)

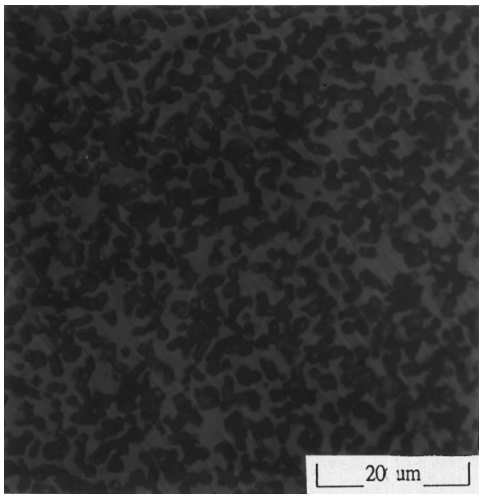

(*b*)

Fig. 7—(*a*) OM observation of composites with various heat treatments for 2 h at 770 °C. (*b*) Enlargement of (a).

The following expression is often referred to as the Johnson–Mehl–Avrami equation, where k and n are time-independent constants for the particular reaction. The constant k is expressible in terms of the rates of nucleation and growth, and n is a number that depends upon the geometry of the growth process.

$$X(t) = 1 - \exp(-kt^n) \quad [3]$$

where $X(t)$ is the fraction transformed as a function of time. Sometimes we derive the reaction fraction from hardness:

$$X(t) = (H_t - H_0)/(H_{\max} - H_0) \quad [4]$$

where H_t is the hardness of the specimen, $H_{\max}$ is the maximum hardness after the reaction is complete, and H_0 is the hardness of a nonreacted specimen.

From Figure 12, the composites exhibit S-shaped curves at all temperatures in hardness testing, and the hardness reaches its maximum value of about 1000 HV at temperatures from 750 °C to 780 °C. In this temperature range, we derive the reaction fraction from the hardness ($H(t)$) and calculate the Johnson–Mehl–Avrami coefficient (n) from Eq. [3], as shown in Figure 13. The value of n in the Avrami equation is $1.5 < n < 2.5$ in the heat-treatment temperature range from 750 °C to 770 °C and is $n > 2.5$ at 780 °C. It is very different from Tsuchitori and Fukunaga's[21] report, which indicated $0.7 < n < 0.75$ in the heat-treatment temperature range from 500 °C to 600 °C. The values of the exponent n are related, in Christian's report,[23] to the particular nucleation conditions. He summarized the value of n that may be obtained in various experimental conditions, for example, a decreasing nucleation rate for $1.5 < n < 2.5$ and an increasing nucleation rate for $n > 2.5$. However, the variation of $X(t)$ with $t^{2/3}$ is valid only for the very early stages of segregation of solute atoms to dislocation. It is apparent that the nucleation and growth processes are different in heat treatments above the liquidus temperature and heat treatments below the liquidus temperature. From the Arrhenius equation, $r = A \exp(-Ea/RT)$, where r is the reaction rate, Ea is the activation energy, and A is the pre-exponential factor. The time-at-reaction fraction ($X = 0.5$) was used as the reaction rate. The overall activation energy of the formation of $TiAl_3$ and Al_2O_3 composites calculated is about 286 kJ/mole, as shown in Figure 14. This value is close to the self-diffusion of O^{2-} in Al_2O_3, which has a 264 kJ/mole activation energy[21] and also to the self-diffusion of O^{2-} in TiO_2, which has an activation energy of 251 kJ/mole. Isao[16] also calculated an activation energy of about 277 kJ/mole in TiO_2/A356. However, the mechanism of the reaction of TiO_2 and Al is still unknown and needs further study.

Owing to the disappearance of Al phase and the generation of $TiAl_3$ and Al_2O_3, the bending strength of composites decreased rapidly from 685 to 154 MPa after heat-treatment, as shown in Figure 11. Li[24] revealed that the presence of $TiAl_3$ decreased the bending strength because of its brittleness. Al_2O_3 was also brittle, as is well known. In addition, from the theoretical calculation of Eq. [1] ($x = 0$), the volume of the $Al_2O_3/TiAl_3$ composite is smaller than that of the TiO_2/A356 composite by about 5 pct. The bending strength of the $Al_2O_3/TiAl_3$ composite was low due to internal pores in the specimen, since the bulk dimension of the specimen did not change. A typical fracture surface of the composite is shown in Figure 15. Al_2O_3 particle clusters were found in the fracture surface of the specimen heat treated above 740 °C and formed a porous region, shown in Figure 15(b). Thus, the bending strength was decreased.

V. CONCLUSIONS

In-situ $Al_2O_3/TiAl_3$ composites were generated from TiO_2/A356 composites *via* heat treatment from 700 °C to 780 °C. The major results may be summarized as follows.

1. The Al matrix composite with 33 vol pct TiO_2 powder was heated above 750 °C (750 °C to 780 °C) and was completely transformed into an $Al_2O_3/TiAl_3$ intermetallic matrix composite.

The reaction is $3\ TiO_2 + 13\ Al \rightarrow 3\ TiAl_3 + 2\ Al_2O_3$.

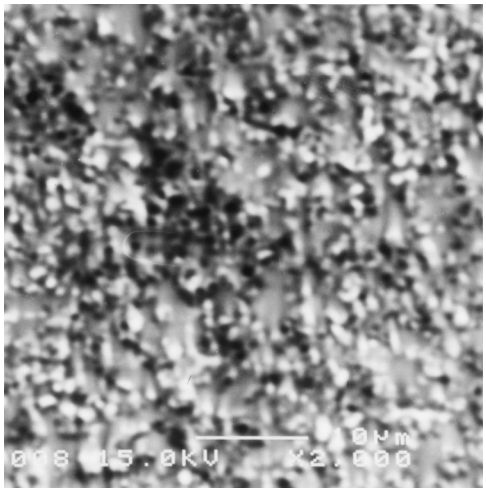

(*a*)

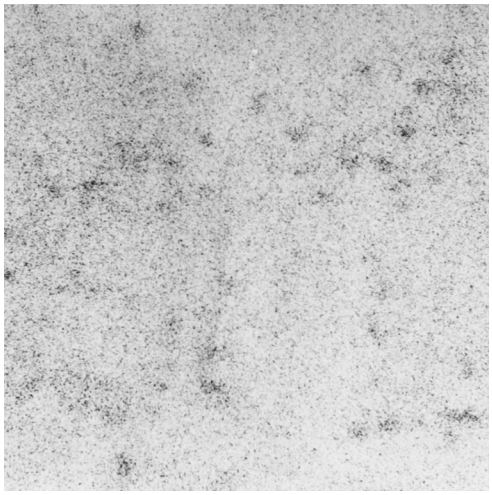

(*b*)

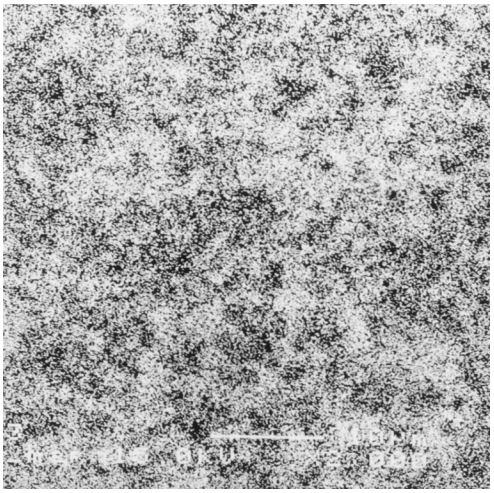

(*c*)

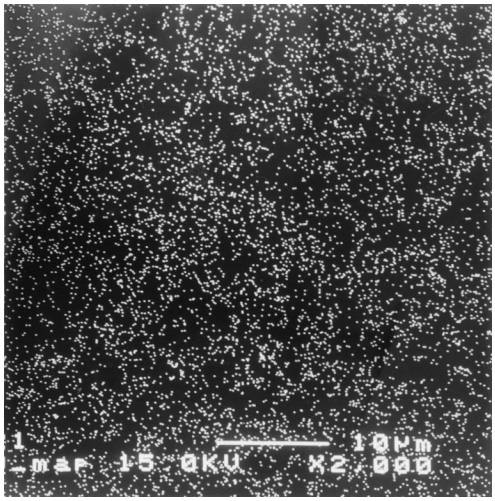

(*d*)

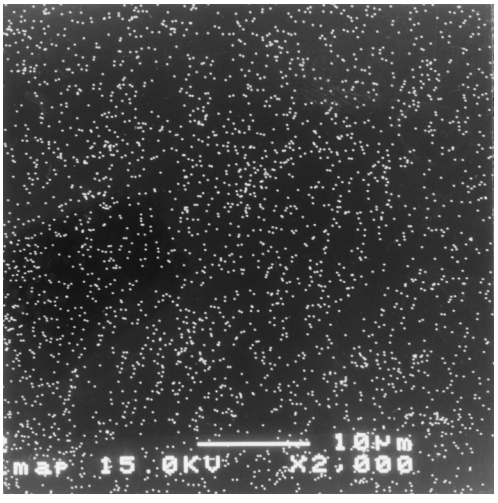

(*e*)

Fig. 8—EPMA of TiO_2/A356 composite heat-treated at 770 °C for 2 h, showing (*a*) electron image of a region and corresponding X-ray images of (*b*) Al, (*c*) Ti, (*d*) O, and (*e*) Si.

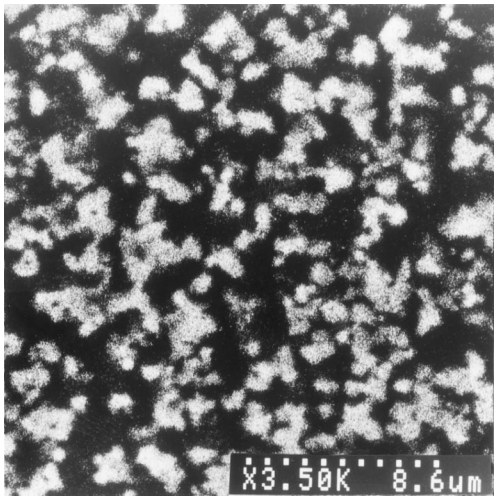

(*a*)

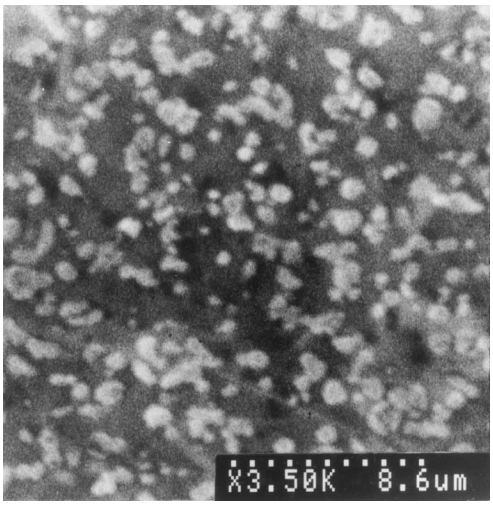

(*b*)

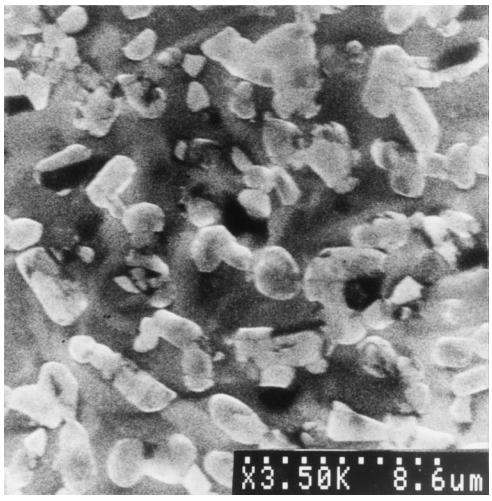

(*c*)

Fig. 9—SEM observations of composites (*a*) as-squeezed and heat-treated at (*b*) 720 °C, (*b*) 740 °C, and (*c*) 760 °C.

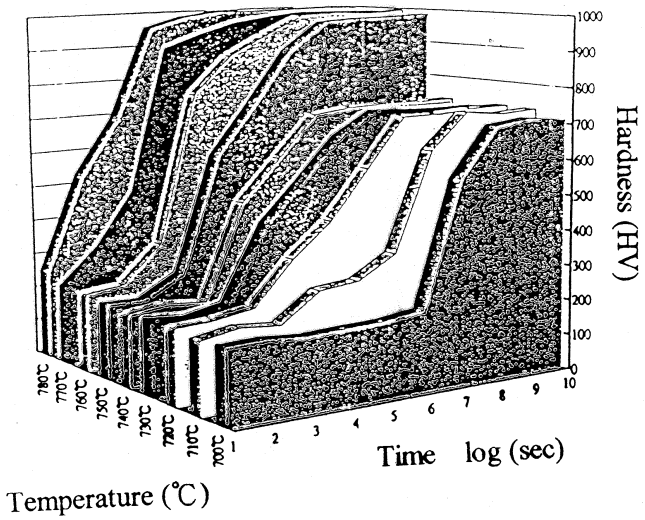

Fig. 10—Pictorial drawing of hardness under different temperatures and time.

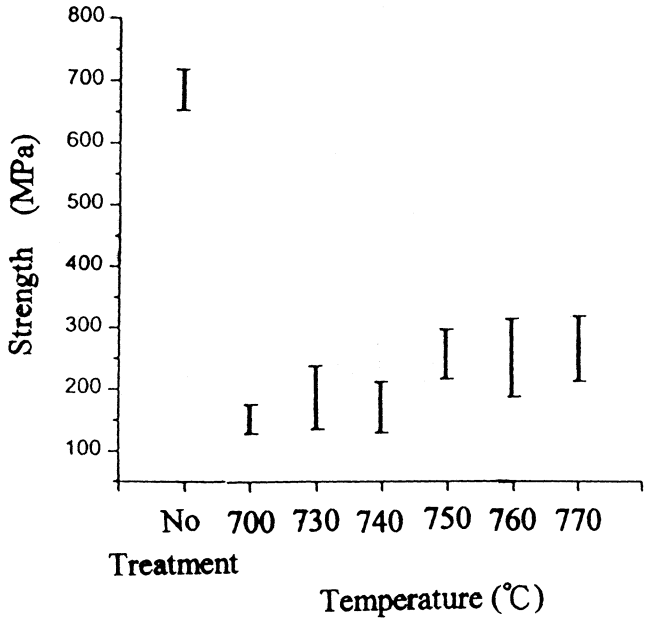

Fig. 11—Bending strength of composites with various heat-treatment temperatures.

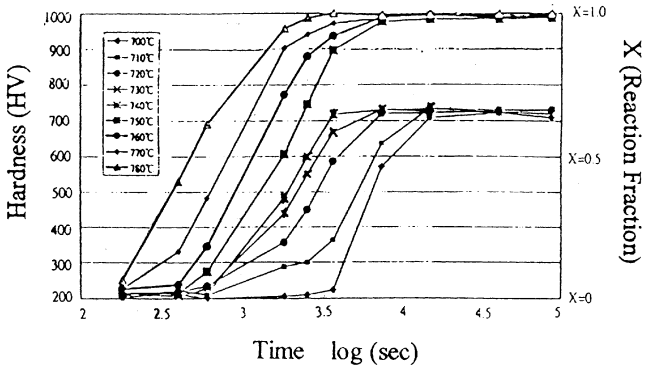

Fig. 12—The relationship between hardness and heat-treatment time with various temperatures.

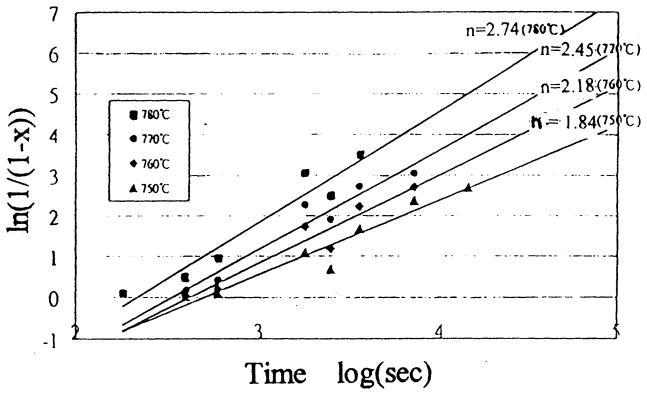

Fig. 13—Johnson–Mehl–Avrami plot of hardening reaction of TiO_2/A356 composite.

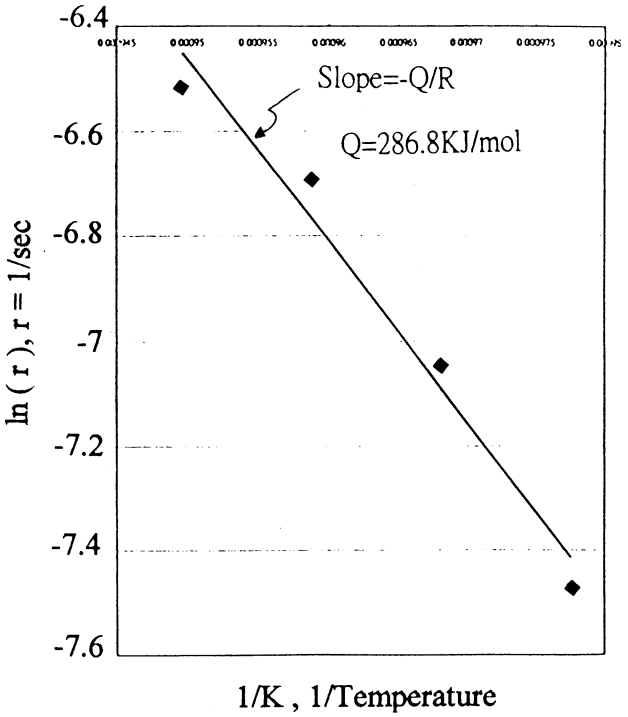

Fig. 14—The activation energies of formation Al_2O_3 and $TiAl_3$ form TiO_2 and A356.

2. The *in-situ* synthesis $Al_2O_3/TiAl_3$ composite formed above 750 °C (750 °C to 780 °C) has high hardness of about 1000 HV. This hardness of $Al_2O_3/TiAl_3$ composite is much higher than that of the specimens (750 HV) heated below 740 °C (700 °C to 740 °C) and of nonreacted TiO_2/A356 composite (200 HV).
3. The bending strength of composites decreases rapidly from 685 to 154 MPa due to porosity occurrence during the formation of Al_2O_3 and $TiAl_3$.
4. In the hardening reaction, the apparent activation energy is 286 kJ/mole.

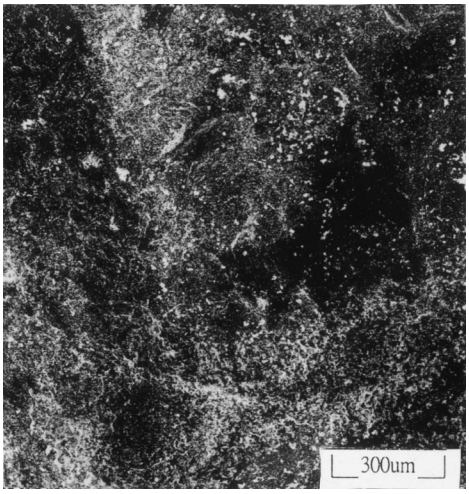

(*a*)

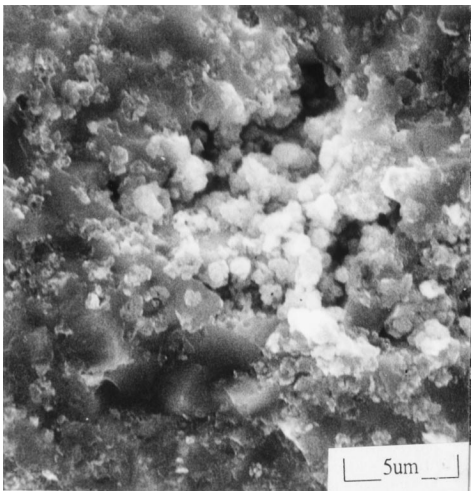

(*b*)

Fig. 15—(*a*) and (*b*) The fracture surface of composite with 760 °C heat treatment.

ACKNOWLEDGMENT

The authors are pleased to acknowledge the financial support of this research by the National Science Council, Republic of China, under Grant No. NSC88-2216-E-009-014.

REFERENCES

1. Terence M.F. Ronald: *Adv. Mater. Proc.*, 1989, vol. 135 (5), pp. 29-37.
2. Y.W. Kim and D.M. Dimiduk: *JOM*, 1991, vol. 43 (8), pp. 40-47.
3. F.H. Froes, C. Suryanarayana, and D. Eliezer: *Iron Steel Inst. Jpn. Int.*, 1991, vol. 31 (10), pp. 1235-48.
4. M.S. DiPietro, K.S. Kumar, and J.D. Whittenberger: *J. Mater. Res.*, 1991, vol. 6 (3), pp. 530-38.
5. S. Mitao, S. Tsuyama, and K. Minakawa: *Mater. Sci. Engr.*, 1991, vol. A143, (1–2), pp. 51-62.
6. D.G. Morris, M.A. Morris, S. Guenter, M. Leboeuf, and G. Hollrigl: *Scripta Metall. Mater.*, 1992, vol. 27 (11), pp. 1645-50.
7. A.O. Kunrath, T.R. Strohaecker, and J.J. Moore: *Scripta Mater.*, 1996, vol. 34 (2), pp. 183-88.
8. H.X. Peng, D.Z. Wang, L. Geng, C.K. Yao, and J.F. Mao: *Scripta Mater.*, 1997, vol. 37 (2), pp. 199-204.

9. N.J. Welham: *Intermetallics*, 1998, vol. 6 (5), pp. 363-68.
10. H. Fukunaga, X. Wang, and Y. Aramaki: *J. Mater. Sci. Lett.*, 1991, vol. 10 (1), pp. 23-35.
11. I. Tsuchitori and H. Fukunaga: *J. Jpn. Inst. Light Met.*, 1993, vol. 43 (1), pp. 26-32.
12. I. Tsuchitori, N. Morinaga, and H. Fukunaga: *J. Jpn. Inst. Met.*, 1995, vol. 59 (3), pp. 331-38.
13. K.C. Chen and C.G. Chao: *Metall. Mater. Trans. A*, 1995, vol. 26A, pp. 1035-43.
14. ASM Handbook Committee: *Metals Handbook*, 9th ed., vol. 8, *Mechanical Testing*, ASM, Metals Park, OH, 1985, p. 136.
15. K. Suganuma, T. Fujita, K. Niihara, and N. Suzuki: *J. Mater. Sci. Lett.*, 1989, vol. 8 (7), pp. 808-10.
16. I. Tsuchitori and H. Fukunaga: *J. Jpn. Inst. Met.*, 1992, vol. 56 (3), pp. 333-41.
17. P.C. Maity, S.C. Panigrahi, and P.N. Chakroborty: *Scripta Metall. Mater.*, 1993, vol. 28 (5), pp. 549-52.
18. D.Z. Wang, Z.R. Liu, C.K. Yao, and M. Yao: *J. Mater. Sci. Lett.*, 1993, vol. 12 (18), pp. 1420-21.
19. Hugh Baker: *Alloy Phase Diagrams*, ASM INTERNATIONAL, Materials Park, OH, 1993, vol. 3, p. 254.
20. H. Okabe: *J. Jpn. Inst. Met.*, 1985, vol. 49 (10), pp. 891-98.
21. I. Tsuchitori and H. Fukunaga: *J. Jpn. Inst. Met.*, 1994, vol. 58 (9), pp. 1029-35.
22. Ira N. Levine: *Physical Chemistry*, 4th ed, McGraw-Hill, 1995, pp. 516-21.
23. J. Christian: *The Theory of the Transformations in Metals and Alloys*, Pergamon, New York, NY, 1965.
24. J.H. Li, X.G. Ning, H.Q. Ye, J. Pan, and H. Fukunaga: *J. Mater. Sci.*, 1997, vol. 32 (2), pp. 543-47.